journal

J. Am. Ceram. Soc., 92 [7] 1580–1585 (2009)
DOI: 10.1111/j.1551-2916.2009.03064.x

Characterization of the Grain-Boundary Character and Energy Distributions of Yttria Using Automated Serial Sectioning and EBSD in the FIB

Shen J. Dillon[‡] and Gregory S. Rohrer[†,§]

[‡]Department of Materials Science and Engineering, University of Illinois, Urbana-Champaign, Urbana, Il 61801

[§]Department of Materials Science and Engineering, Carnegie Mellon University, Pittsburgh, Pennsylvania 15213-3890

A dual-beam focused ion beam scanning electron microscope was used to collect a series of parallel electron backscatter diffraction maps of polycrystalline yttria. Using characteristics of the triple junctions, the individual layers were aligned and the geometries of the grain-boundary planes between the layers were determined. This information was used to calculate the five-parameter grain-boundary character distribution (GBCD) and grain-boundary energy distribution (GBED). The GBCD derived from the three-dimensional data was qualitatively the same as that derived from a stereological analysis of the same data. The anisotropy in the GBCD of yttria is relatively weak compared with other ceramics and is inversely correlated to the GBED.

I. Introduction

Grain boundaries play an important role in the processing and properties of virtually all polycrystalline materials. For example, grain growth,[1] deformation,[2,3] fracture,[4] oxidation,[5] corrosion,[6] creep,[7] and sintering[8] are all influenced by grain boundaries. The structures, properties, and energies of individual grain boundaries vary significantly as a function of lattice misorientation and grain-boundary plane orientation.[9] Therefore, there is interest in characterizing the relative populations and properties of grain boundaries as a function of these crystallographic parameters. The five-parameter grain-boundary character distribution (GBCD) specifies the relative areas of grain boundaries, classified according to the three lattice misorientation parameters and the two grain-boundary plane orientation parameters.[10] In parallel with the GBCD, one can define the grain-boundary energy distribution (GBED) that specifies the relative energies of grain boundaries according to the same five crystallographic parameters. Results of experiment and simulation indicate that there is an inverse correlation between the GBCD and GBED such that lower-energy boundaries are more populous than higher-energy boundaries.[11–21] However, because of the significant experimental challenges associated with determining the five-parameter GBED, there is only a single comprehensive measurement.[12] The main challenge is that the measurement requires a vast amount of data specifying the three-dimensional (3D) geometry of triple junctions. The purpose of the current paper is to show that this challenge can be overcome by using automated serial sectioning in the dual-beam focused ion beam (FIB).

Saylor *et al.*[12] reported the first comprehensive experimental study of the GBED. This was accomplished by collecting electron backscatter diffraction (EBSD) data from calibrated serial sections of magnesia produced by manual polishing. Grain-boundary traces from parallel layers were measured from thermal grooves observed in the scanning electron microscope. Corresponding grains in adjacent layers were identified and connected so that the interface and triple junction geometries could be determined. Assuming local equilibrium at the triple junctions, the Herring[22] condition is satisfied and an equilibrium equation was written for each observed triple junction. The method of Moraweic[23] was then used to find a set of grain-boundary energies that most closely satisfies all of the observed equations. Because the manual polishing and data acquisition are both laborious and difficult, similar measurements have not been repeated often. This method was used with a smaller amount of data to characterize a subset of GBED of a lead–tin alloy.[20] The limited use of this technique likely stems from the difficulty of acquiring accurate, 3D geometric data.

The development of the dual-beam FIB scanning electron microscope (SEM) provides an opportunity to collect calibrated serial sections of images or EBSD maps on a more routine basis through an automated process. The ability of this technique to show the 3D geometry of a microstructure has already been demonstrated in a number of metals and ceramics, but neither the GBCD or GBED have been determined from such data.[24–26] Applying this technique to metallic systems appears to be straight forward. However, ceramic systems present several obstacles to collecting serial sections of EBSD data by FIB. Electrically insulating ceramics are prone to charging, especially during the relatively long acquisition times required for collecting EBSD maps. The high bond-strength of many ceramic materials causes ion-milling rates to be slow. It is also necessary to optimize the milling parameters such that beam damage does not significantly affect the EBSD patterns. This paper describes a method to combine the geometric information from serial sectioning with the crystallographic EBSD data and calculate both the GBCD and GBED. The technique is applied to polycrystalline yttria, an important laser host material.[27] Yttria has the bixbyite structure and little is known about the grain-boundary energetics of materials with this crystal structure.

II. Experimental Procedure

Undoped yttria (MetaMateria Partners, Columbus, OH) was cold isostatically pressed and then sintered at 1500°C for 4 h in air. Two sets of samples were prepared; one for stereological analysis[28] and another for 3D FIB-SEM. A bulk sample for stereological analysis was polished to a 1 μm diamond finish and then coated with a thin film of carbon to prevent charging in the SEM. The second set was polished such that they had two perpendicular polished faces; one to be milled and scanned and the other to provide a square edge for consistent ion milling. The samples were sputter coated with ~2 nm of platinum and "glued" onto a 45° pretilted stub using conductive carbon paint. On a 45° pretilted stub, the sample may be tilted 7° toward the ion beam in the FIB (Nova 600, FEI Co., Hillsboro, OR), or

E. Dickey—contributing editor

Manuscript No. 25164. Received August 27, 2008; approved March 7, 2009.
[†]Author to whom correspondence should be addressed. e-mail: gr20@andrew.cmu.edu

rotated 180° and tilted 25° toward the EBSD detector for data collection (EDAX, Mahwah, NJ). It is essential that a continuous coating of electrically conductive material surrounds the area of analysis in order to prevent charging. The high-tilt angle of the sample also helps to reduce charging by increasing the back-scatter yield.

Circular fiducial markers were milled into the samples and, during the automated data collection, were used to align the area of interest during subsequent milling and EBSD mapping steps. It is important that the sample be well-aligned so that the amount of material milled away in each step is consistent and controlled. Alignment is also important to ensure that the EBSD maps are being collected from the same region in subsequent steps. Automation of the procedure was performed using control scripts in the FEI runscript language.

The sample was ion-milled at 30 kV and 7 nA using a Ga^+ ion beam. EBSD data were acquired using a 30 kV beam at a current of 9.5 nA. The slice thickness between subsequent serial sections was 280 nm, and the in-plane resolution of the EBSD scans was 70 nm. The scan area for each of these samples was approximately 30 μm × 40 μm. The area-weighted average grain size of each sample was 2.5 μm. The number of distinct grains observed was approximately 3600. The EBSD patterns were binned to 4 × 4 and collected at approximately 150 points per second. The EBSD data were cleaned using two iterations of grain dilation (TexSEM, EDAX) with a minimum grain size of 10 pixels. This procedure considers any grouping of <10 pixels, with disorientations of $>5°$, to be insufficient to define a single grain and assigns their orientation to match the orientation of an adjacent grain. A single average orientation was assigned to each grain, with an individual grain being defined as a set of pixels whose disorientations lie within 5° of one another. The cleaned data were aligned using a commercially available 3D OIM visualization software (EDAX). This software uses a cross correlation between the three different color channels in the orientation image map to produce the best alignment on a fixed grid; we refer to this as primary alignment. Grain-boundary line segments were extracted from each slice using commercially available software (EDAX). The maximum deviation between the actual boundary position and the line segment is two pixels.

The line segments from each layer were then processed by software written in house. The first step was to identify the triple points. Any three line segments on a common layer that share a single endpoint were designated as belonging to a triple junction. Each triple junction was then compared with the five closest triple junctions on a parallel layer. If the disorientations between the three grains in the first junction and three grains around one of the five closest junctions were $<5°$, then it was assumed that the triple points on the two layers are connected by a triple line. This is illustrated in Fig. 1. Each of the three line segments define vectors tangent to grain-boundary planes (t_i) and the triple line defines a vector within each of the three grain-boundary planes (l). Therefore, direction of the cross product of t_i and l gives the orientations of the grain-boundary planes (n_i) and one half of the magnitude of the cross product gives the areas of the triangles defined by t_i and l. A second set of normal vectors and triangles was similarly defined from the three tangents on the second plane. Only grain-boundary segments adjacent to triple junctions were analyzed. The vast majority of grain boundaries were composed of one or two reconstructed grain-boundary segments. Less than 2% of the grain-boundary segments were excluded from the analysis because they lie between two other reconstructed grain-boundary segments.

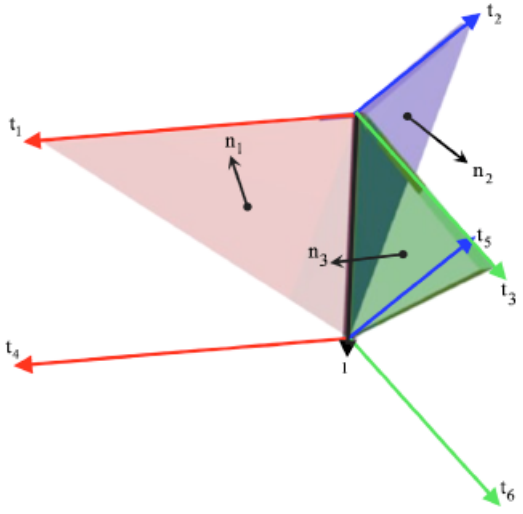

Fig. 1. Schematic of a triple junction showing how the relevant grain-boundary planes are defined.

One important source of uncertainty that derives from the discrete nature of the data is related to the relative in-plane (horizontal) and between planes (vertical) resolution. The actual location of a triple junction or grain boundary must lie within one of the pixels defining the boundary. Therefore, the boundary defined in the EBSD map approximates the actual location of the boundary. It is possible to calculate a maximum error associated with determining the location of the boundary plane by assuming that the actual location of the boundary may vary by up to one pixel. For example, on a fixed grid with points equally spaced in the horizontal and vertical directions, the triple line must take discrete orientations. The maximum angular separation between these orientations occurs for the direction aligned parallel to the sample normal and the one inclined 45° to the sample normal, connecting the nearest point on the next layer. For this case, the maximum error is 45°. In this work, we used a horizontal grid spacing that was one quarter the vertical grid spacing, reducing the maximum error to 14°. This error is slightly larger than the binning used (10°), however, because this is a maximum error it is expected that majority of the data will lie in the appropriate bin. These errors result in boundaries that have a "zig-zag" structure through the microstructure. Because the majority of these "zig-zag" structures fall within binning resolution, the errors associated with their specific geometric variations are small.

A second important source of uncertainty is related to the horizontal alignment of the layers. Because the sample was tilted and rotated during each subsequent data collection step it is difficult to perfectly realign the sample before EBSD acquisition. The EBSD data were collected on a fixed grid, but misalignments at resolutions lower than the pixel size may still introduce significant errors. Subpixel alignments may essentially minimize the errors discussed at the end of the previous paragraph. An analysis of the distribution of triple line directions indicated the need for such a refined subpixel alignment. Considering the equiaxed nature of the microstructure, it was assumed that the triple line directions should be randomly distributed around the sample's normal direction. The scatter plot in Fig. 2(a) shows the distribution of the in-plane components of the triple line vectors for two representative layers. The mean of this distribution is in the upper right-hand quadrant of the distribution. To move the mean to the position of the normal, a rigid shift was applied to the in-plane coordinates. This was repeated for each pair of layers and we refer to this as secondary alignment. The shifts applied to each layer are shown in Fig. 2(b). The shifts were all smaller than the slice thickness and the majority of the data are horizontally shifted by $<$two pixels. Note that the required shifts in the x-direction (fast scan direction) tend to be smaller than in the y-direction. After secondary alignment, the endpoints of the vectors defining the grain-boundary tangents and triple lines were no longer confined to a fixed 3D grid.

3D orientation maps, needed for input into visualization software, were created in the following way. First, grains on individual layers were assigned identification numbers and the mean position of each grain was calculated. The data from each layer was then compared and, if two grain sections on different layers had a disorientation $<3°$ and a mean position separated by less

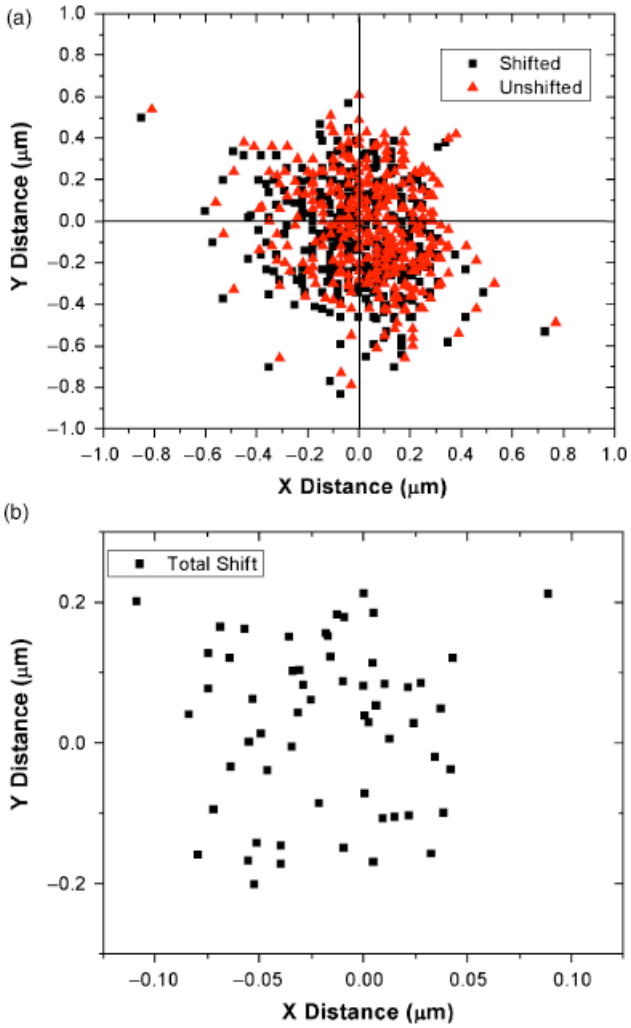

Fig. 2. (a) A scatter plot of the x and y components of the triple line vectors between two data slices showing the shifted and unshifted data and (b) the total x, y shift between each slice of data.

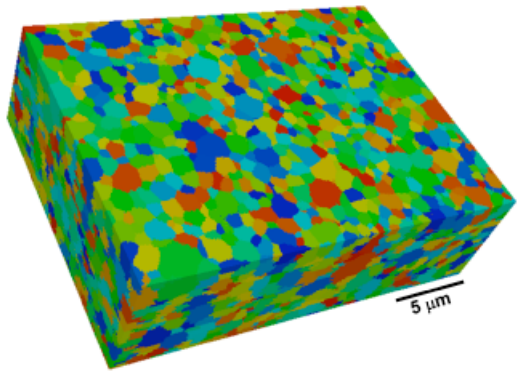

Fig. 3. Reconstructed serial sections of electron backscatter diffraction data from undoped yttria. The data contains 43 of the 63 slices collected in this study.

than two mean grain diameters, they were assigned the same grain identification number.

The GBCD was calculated from the extracted triangles using the methods described previously.[11] Briefly, the five-parameter space is discretized into equal volume bins spanning approximately 10° in each parameter. Each triangular area was placed in the bin corresponding to its misorientation and boundary orientation, and all of the symmetrically equivalent bins. There were 141 000 triangles and 99.4% of the bins in the discretized GBCD contained at least 10 triangles. The areas in each bin were then normalized by the average area per bin so that the distribution has units of multiples of a random distribution (MRD). For comparison, the GBCD was also calculated using stereological principles. In this case, the 141 000 line segments from the parallel slices were used as input and calculation was carried out exactly as described in Saylor *et al.*[28] This analysis was also performed using 110 000 line segments obtained from ~36 000 grains in single planar section of the sample. The stereological analysis of a single planar section was performed, for comparison, to ensure that the 3D volume of data was representative of a larger population of grains within the sample. As a control, several different sets of 140 000 randomly generated triangles were produced to establish the amount of anisotropy observed when the same procedures are applied to a random distribution. In order to quantitatively compare the stereologically derived GBCD with the one obtained from serial sectioning, the serial-sectioned data were binned into 0.2 MRD wide bins. The corresponding points in the 5D space of the stereological data were averaged together for comparison.

The GBED was calculated using the method described by Moraweic (see reference for details of analysis and associated errors).[23] The data set contained 47 000 triple junctions and the calculation used a relaxation factor of 0.05. After 400 iterations, adjustments to the capillarity vector field were $<1\%$ of the initial adjustment and it was assumed that the calculation converged. It was confirmed that the value of the relaxation factor did not affect the results as long as the process was convergent. The final result was smoothed by averaging the capillarity vectors in neighboring bins, as described previously.[12]

III. Results

Figure 3 shows 3D reconstructed data for yttria. For the purposes of visualization, only the primary alignment procedure in the commercial software was used. This provides a reasonable reconstruction and is an acceptable starting point for the reconstruction of the grain-boundary planes.

The efficacy of the secondary, subpixel alignment procedure is demonstrated in Fig 4. The distribution of grain-boundary planes in the bicrystal reference frame for misorientations of 30° and 60° rotations about [111] are shown in Figs. 4(a) and (b) when only the primary alignment procedure is used. This can be compared with the same sections in Figs. 4(c) and (d), calculated after the secondary alignment procedure. In each distribution, there is a peak at the twist position, where the grain boundary is bounded on both sides by a (111) plane. However, the amplitudes of the distributions produced by the secondary alignment procedure are greater (by 15%) than those produced by the primary alignment. This is because the maximum error in the triple line position after primary alignment (14°) exceeds the average bin size (10°) and a larger fraction of the boundary planes are incorrectly classified if the secondary alignment is not used. The maximum peak at any point in the distribution calculated from randomly generated triangles was 1.6 MRD. Any peaks larger than this may be interpreted as real features of the distribution.

For comparison, the same distributions calculated using the stereological analysis, on the same grain-boundary line segments from serial section data, are shown in Figs. 4(e) and (f). The stereological analysis was also performed on data from a single planar section and the results were similar to the analysis performed on serial sections. This indicates that our 3D volume is a representative sample of the general microstructure. The distributions, calculated from stereology and the reconstructed volume, are qualitatively identical, but the anisotropy calculated using the stereological methods is greater than that from the 3D analysis. The GBED for the same misorientations are shown in Figs. 4(g) and (h). The energy shows an approximate inverse relationship to the distribution; the minimum energy occurs at

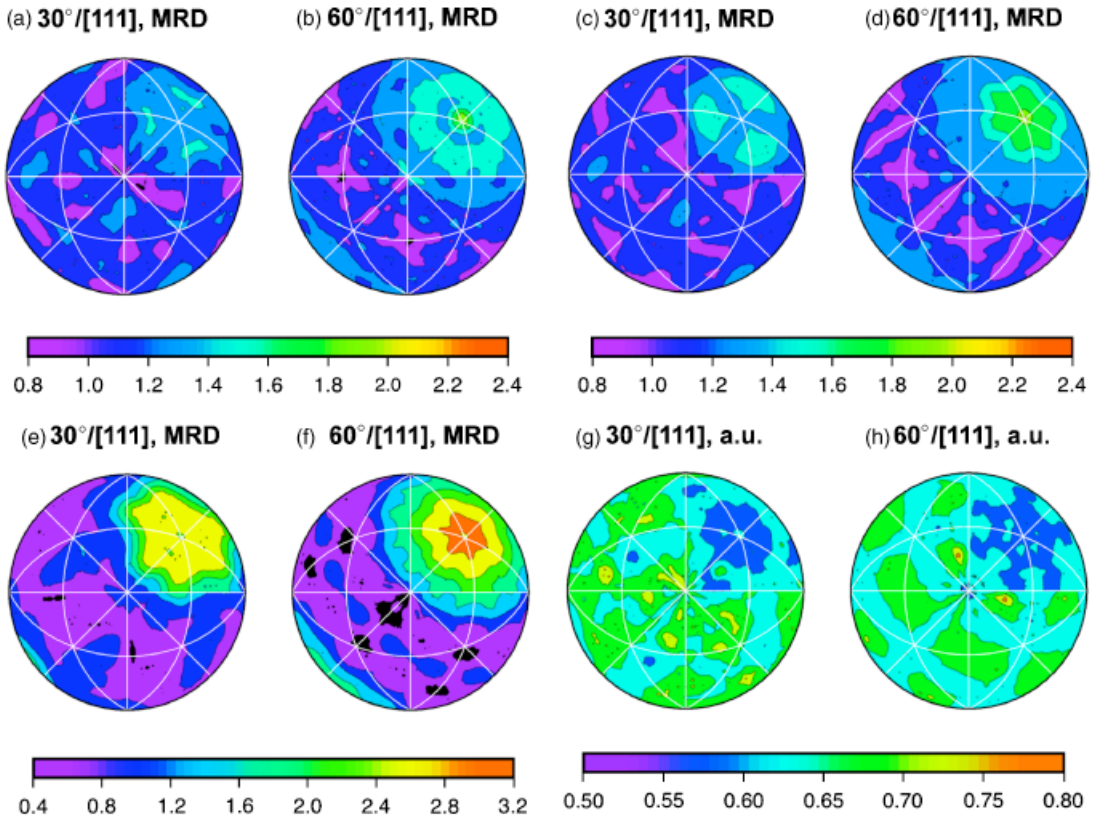

Fig. 4. (a–f) The grain-boundary plane distribution at the fixed misorientations of 30°/[111] and 60°/[111], plotted in stereographic projection along [001]. The distributions calculated after primary alignment are shown in (a) and (b). The distributions calculated after secondary alignment are shown in (c) and (d). The stereologically calculated distributions are shown in (e) and (f). The corresponding energy distributions are shown in (g) and (h).

the (111) twist position where the grain-boundary plane distribution reaches a maximum. The difference in anisotropy in the GBCD may be observed quantitatively in the plot in Fig. 5. This plots the average MRD of corresponding bins in the GBCDs derived from serial sectioning and stereology. Ideally, there would be a one-to-one correlation (solid line in Fig. 5) but the reduced slope indicates that the data calculated from serial sections is less anisotropic. However, the fact that the slope of this correlation is approximately linear indicates that the distributions display the same trend. Figures 6(a)–(d) show the GBCD for misorientations about the [110] and [111] axes, with the corresponding energy distributions shown in Figs. 6(e)–(h). The distribution of grain-boundary plane normals, independent of misorientation, and their relative energies are plotted in Figs. 7(a) and (b), respectively.

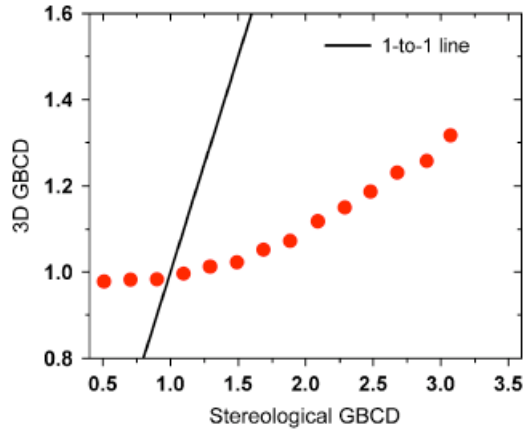

Fig. 5. The relationship between equivalent bins in the grain-boundary character distributions of the stereological and three-dimensional (3D) data.

IV. Discussion

The maximum in the GBCD occurs for the 60°/[111] pure twist boundary and is 2.4 or 3.2 MRD, based on the 3D and stereological results, respectively. This is one of the weakest anisotropies that has been reported.[29] The quantitative differences between the 3D analysis and the stereology are not understood at this time. Modeling of the stereological analysis suggests that maxima are systematically underestimated. Because the 3D analysis produces peaks that are lower than the stereology result, it seems likely that some uncertainty is added in the calculation of the grain-boundary normals and that this places some observations in the bins neighboring their true position, making the peaks broader and less intense. Note that stereology and the 3D analysis shown use exactly the same in plane line segments as input. Therefore, the uncertainty introduced in the 3D analysis must derive from the correlations between the layers. Quantifying and reducing these uncertainties will be the subject of future investigations. While the peaks in the GBCD are relatively low as compared with some previously studied oxides,[29] they are significantly greater than those occurring in a random distribution. Therefore, the current results give a reasonable representation of the true GBCD and it is encouraging that the features of even a highly isotropic distribution can be clearly distinguished. While the 3D analysis underestimates the anisotropy in the GBCD, it may be preferred over the stereological analysis in cases where it is important to characterize the local behavior, when crystallographic texture affects the stereological analysis, or it is critical to collect both the GBCD and the corresponding GBED.

Misorientations about the [100] are highly isotropic having no peaks in the distribution that occur with frequencies greater than random. Therefore, a relationship between the GBCD and GBED at these boundaries is not expected. Larger than expected variations in the GBED within this isotropic range might occur as a result of under sampling of certain low-frequency

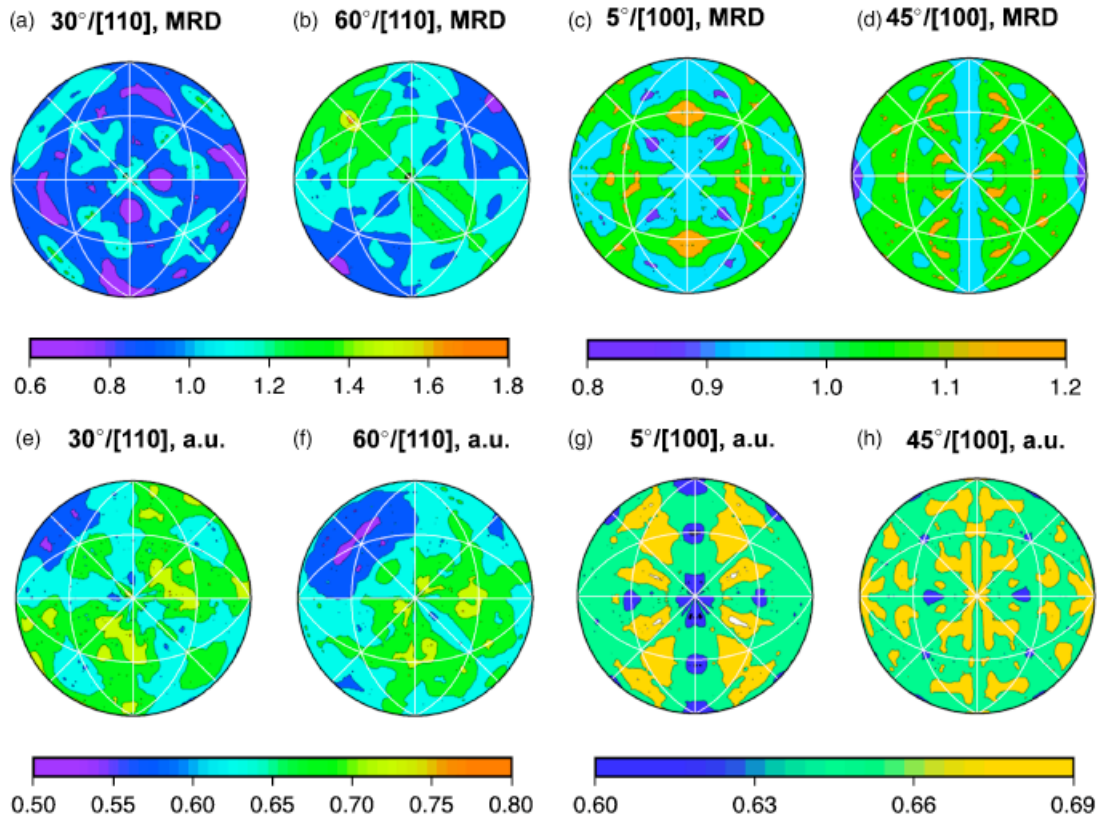

Fig. 6. (a–d) The grain-boundary plane distribution at the fixed misorientations of 30°/[110], 60°/[110], 5°/[100], and 45°/[100], respectively, plotted in stereographic projection along [001]. (e–h) The corresponding grain-boundary energy distribution at the fixed misorientations of 30°/[110], 60°/[110], 5°/[100], and 45°/[100], respectively, plotted in stereographic projection along [001].

boundaries. There is a major peak in the distribution at 60° about the [110] with grain boundaries formed by (111) planes (near twist boundaries). This boundary is likely emphasized due to its proximity to the coherent Σ3 (70.53°/[110] is symmetrically equivalent to 60°/[111]).

One of the most interesting results of the previous work was the recognition that there is an inverse relationship between the grain-boundary energy and grain-boundary population.[11,12] This relationship has also been confirmed by simulation.[15,16] The results from this study show the same behavior; the most populous grain boundaries are also the lowest energy grain boundaries. On the other hand, careful inspection of Figs. 4, 6, and 7 shows that there is not a strict one-to-one relationship between energy and population. While a perfect inverse correlation is not necessarily expected, the calculation of the relative energies is affected by the same uncertainties that influence the GBCD. Despite this, the previously observed inverse relationship between population and energy is clearly reproduced in yttria.

Magnesia, which has the rocksalt structure, has been found to be relatively anisotropic with relatively low-energy (100) planes and relatively high-energy (111) planes.[12] Figures 7(a) and (b) indicate the opposite with respect to yttria, which has relatively high-energy (100) planes and relatively low-energy planes near (111). The common feature is that in both systems the high-energy planes terminate either entirely in anions or cations (see schematics in Fig. 8). Alternatively, their low-energy planes are terminated in a manner that accommodates both anions and cations. Charge neutrality must be maintained across a grain boundary and it is not favorable to form cation–cation or anion–anion bonds. For example, if a grain boundary is composed of a plane that terminates entirely by cations and another terminated by mixed ions, then there will be a large number of cation–cation neighbors that will be energetically unfavorable. This could be remedied by introducing vacancies; however, other charged defects would be needed to compensate the vacancies. These arguments suggest an explanation for the com-

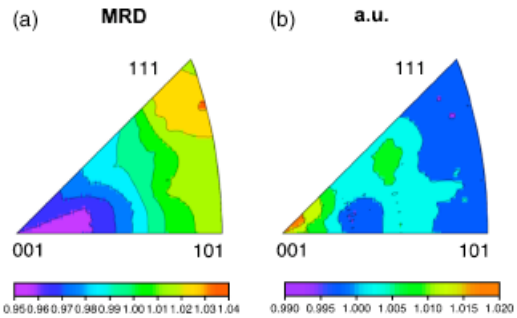

Fig. 7. (a) The distribution of grain-boundary plane normals, independent of misorientation, in yttria and (b) the corresponding average energies.

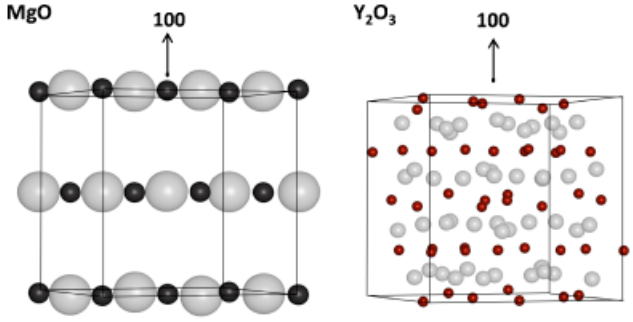

Fig. 8. Schematics of the yttria and magnesia crystal structures. In both schematics the larger circles (light gray) are the oxygen and the smaller circles are the cations (Mg is black and Y is red).

mon features of grain-boundary energetics between magnesia and yttria.

The major difference between magnesia and yttria is the magnitude of the anisotropy. It is suspected that magnesia may be more anisotropic due to its larger variations in planar atomic packing density, especially with respect to the presence of high-density close-packed planes. The bixbyite structure is a body-centered cubic type structure (Ia-3), which has no close-packed plane. While it is difficult to draw broad conclusions based upon the limited available data, it is interesting to note that the GBCD of other body-centered cubic structures characterized (BCC iron and yttrium aluminum garnet) are also relatively isotropic.[30–31]

The isotropic nature of the GBED and GBCD in yttria produce the equiaxed grain structure typically observed in this system.[27] This type of distribution is not likely to produce a bimodal grain size distribution, because any discontinuous changes in grain-boundary structure, energy, mobility, or composition are not likely to be confined to a small fraction of grain boundaries, but rather occur throughout the microstructure. This behavior makes yttria an ideal system for sintering to high density, because pore-boundary separation is unlikely to occur to any large extent. Grain-boundary segregation is also likely to be isotropic, because there are often correlations between energy anisotropy and segregation anisotropy.[13] This understanding is useful for designing doping strategies or approaches to microstructural control. For example, this behavior may be advantageous for producing polycrystalline laser hosts for high-power applications, where strong local variations in composition at grain boundaries might adversely affect optical properties. The isotropic nature of interfacial energetics in this system may also extend to surfaces, which would be beneficial to the stability of various crystallographic planes on single crystals or epitaxial films. Random surfaces in highly anisotropic systems often decompose into sets of lower energy orientations.

Automated collection of calibrated serial sections using the dual-beam FIB has opened up new possibilities for characterizing the grain-boundary network in detail. What was once a laborious data collection process has now been reduced to a routine procedure. Collection times for data have been reduced to a few hours or days rather than a few weeks or months. The inverse correlation between energy and population previously observed in magnesia has been conformed for yttria, although yttria is much less anisotropic both in the GBCD and GBED. Continued effort to improve the resolution and meshing of the interfaces is expected to improve the accuracy of the boundary plane and energy distributions.

V. Conclusions

Both the GBCD and the GBED can be derived from serial section EBSD maps obtained in the dual-beam FIB-SEM. This GBCD is qualitatively the same as derived from a stereological analysis of the identical data. Although the 3D analysis underestimates the anisotropy, it offers the ability to characterize site-specific distributions and interfacial distributions in textured materials. The GBED is inversely correlated to the GBCD, which is consistent with earlier work in magnesia. Polycrystalline yttria displays weak anisotropy. This may arise from the absence of close packed planes in yttria. The results suggest that planes terminated entirely by a single type of ion tend to be high energy. The automated data collection and analysis procedures described here will permit the routine measurement of the GBCD and GBED for polycrystalline materials.

Acknowledgments

We would like to thank Shuailei Ma and Martin Harmer for providing a well-prepared, dense polycrystalline yttria sample for us to analyze. We would also like to acknowledge the Pennsylvania Department of Community and Economic Development and the MRSEC program of the National Science Foundation, under Award Number DMR-0520425, for their support.

References

[1]J. E. Burke and D. Turnbull, "Recrystallization and Grain Growth," *Progr. Metal Phys. (Interscience Publishers Inc.)*, **3**, 220–92 (1952).
[2]E. O. Hall, "The Deformation and Ageing of Mild Steel: III Discussion of Results," *Proc. Phys. Soc. Lond. Q4*, **Sect. B 64**, 747–53 (1951).
[3]N. J. Petch, "The Cleavage Strength of Polycrystals," *J. Iron Steel Inst.*, **174**, 25–8 (1953).
[4]T. Watanabe and S. Tsurekawa, "Toughening of Brittle Materials by Grain Boundary Engineering," *Mater. Sci. Eng., A: Struct. Mater.: Properties, Microstruct. Process.*, **A387–A389**, 447–55 (2004).
[5]P. Y. Hou, "Impurity Effects on Alumina Scale Growth," *J. Am. Ceram. Soc.*, **86** [4] 660–8 (2003).
[6]M. Shimada, H. Kokawa, Z. J. Wang, Y. S. Sato, and I. Karibe, "Optimization of Grain Boundary Character Distribution for Intergranular Corrosion Resistant 304 Stainless Steel by Twin-Induced Grain Boundary Engineering," *Acta Mater.*, **50** [9] 2331–41 (2002).
[7]R. L. Coble, "A Model for Boundary Diffusion Controlled Creep in Ceramic Materials," *J. Appl. Phys.*, **34**, 1679–82 (1963).
[8]R. L. Coble and J. E. Burke, "Sintering in Crystalline Solids," *Proc. Intern. Symp. Reactivity Solids, 4th, Amsterdam*, **1960**, 38–51 (1961).
[9]A. P. Sutton and R. W. Balluffi, "Overview no. 61 On Geometric Criteria for Low Interfacial Energy," *Acta Metall.*, **35** [9] 2177–201 (1987).
[10]C. Goux, "Grain Boundary Structures: Crystallographic Parameters and Methods for Calculating Structures," *Can. Metall. Q.*, **13** [1] 9–31 (1974).
[11]D. M. Saylor, A. Morawiec, and G. S. Rohrer, "Distribution of Grain Boundaries in Magnesia as a Function of Five Macroscopic Parameters," *Acta Mater.*, **51** [13] 3663–74 (2003).
[12]D. M. Saylor, A. Morawiec, and G. S. Rohrer, "The Relative Free Energies of Grain Boundaries in Magnesia as a Function of Five Macroscopic Parameters," *Acta Mater.*, **51** [13] 3675–86 (2003).
[13]Y. Pang and P. Wynblatt, "Effects of Nb Doping and Segregation on the Grain Boundary Plane Distribution in TiO_2," *J. Am. Ceram. Soc.*, **89** [2] 666–71 (2006).
[14]D. M. Saylor, B. El Dasher, Y. Pang, H. M. Miller, P. Wynblatt, A. D. Rollett, and G. S. Rohrer, "Habits of Grains in Dense Polycrystalline Solids," *J. Am. Ceram. Soc.*, **87** [4] 724–6 (2004).
[15]J. Gruber, D. C. George, A. P. Kuprat, G. S. Rohrer, and A. D. Rollett, "Effect of Anisotropic Grain Boundary Properties on Grain Boundary Plane Distributions During Grain Growth," *Scripta Mater.*, **53** [3] 351–5 (2005).
[16]G. S. Rohrer, J. Gruber, and A. D. Rollett, "A Model for the Origin of Anisotropic Grain Boundary Character Distributions in Polycrystalline Materials"; pp. 343–54 in: *Applications of Texture Analysis*, Edited by A.D. Rollett. Ceram. Trans., 201, J. Wiley & Sons, Hoboken, NJ, 2009.
[17]G. N. Hassold, E. A. Holm, and M. A. Miodownik, "Accumulation of Coincidence Site Lattice Boundaries During Grain Growth," *Mater. Sci. Technol.*, **19** [6] 683–7 (2003).
[18]E. A. Holm, G. N. Hassold, and M. A. Miodownik, "On misorientation Distribution Evolution During Anisotropic Grain Growth," *Acta Mater.*, **49** [15] 2981–91 (2001).
[19]U. Upmanyu, G. N. Hassold, A. Kazaryan, E. A. Holm, Y. Wang, B. Patton, and D. J. Srolovitz, "Boundary Mobility and Energy Anisotropy Effects on Microstructural Evolution During Grain Growth," *Interface Sci.*, **10**, 201–16 (2002).
[20]D. J. Rowenhorst and P. W. Voorhees, "Measurements of Grain Boundary Energy and Anisotropy in Tin," *Metall. Mater. Transact. A*, **36A**, 2127–35 (2005).
[21]D. Kinderlehrer, I. Livshits, G. S. Rohrer, S. Ta'asan, and P. Yu, "Mesoscale Simulation of the Evolution of the Grain Boundary Character Distribution," *Mater. Sci. Forum*, **467–470**, 1063–8 (2004).
[22]C. Herring, "Some Theorems on the Free Energies of Crystal Surfaces," *Phys. Rev.*, **82** [1] 87–93 (1951).
[23]A. Morawiec, "Method to Calculate the Grain Boundary Energy Distribution over the Space of Macroscopic Boundary Parameters from the Geometry of Triple Junctions," *Acta Mater.*, **48** [13] 3525–32 (2000).
[24]J. Konrad, S. Zaefferer, and D. Raabe, "Investigation of Orientation Gradients Around a Hard Laves Particle in a Warm-Rolled Fe_3Al-Based Alloy Using a 3D EBSD-FIB Technique," *Acta Mater.*, **54** [5] 1369–80 (2006).
[25]M. D. Uchic, M. A. Groeber, D. M. Dimiduk, and J. P. Simmons, "3D Microstructural Characterization of Nickel Superalloys via Serial-Sectioning Using a Dual Beam FIB-SEM," *Scripta Mater.*, **55** [1] 23–8 (2006).
[26]L. Holzer, B. Muench, M. Wegmann, P. Gasser, and R. J. Flatt, "FIB—Nanotomography of Particulate Systems—Part I: Particle Shape and Topology of Interfaces," *J. Am. Ceram. Soc.*, **89** [8] 2577–85 (2006).
[27]H. Mingsheng, L. Jianbao, L. Hong, G. Gangfeng, and L. Long, "Fabrication of Transparent Polycrystalline Yttria Ceramics by Combination of SPS and HIP," *J. Rare Earths*, **24** [1, Suppl. 1] 222–4 (2006).
[28]D. M. Saylor, B. S. El-Dasher, B. L. Adams, and G. S. Rohrer, "Measuring the Five-Parameter Grain-Boundary Distribution from Observations of Planar Sections," *Metall. Mater. Transact. A: Phys. Metall. Mater. Sci.*, **35A** [7] 1981–9 (2004).
[29]G. S. Rohrer, D. M. Saylor, B. S. El-Dasher, B. L. Adams, A. D. Rollett, and P. Wynblatt, "The Distribution of Internal Interfaces in Polycrystals," Zeitschrift fur Metallkunde, **95**, 197–214 (2004).
[30]T. A. Bennett, C.-S. Kim, G. S. Rohrer, and A. D. Rollett, "Five-Parameter Grain Boundary Character Distribution in Fe–1%Si," *Mater. Sci. Forum*, **467–470**, 727–32 (2004).
[31]S. J. Dillon and G. S. Rohrer, "Mechanism for the Development of Anisotropic Grain Boundary Character Distributions During Normal Grain Growth," *Acta Mater.*, **57** [1] 1–7 (2009). □